Pergamon

Int. J. Heat Mass Transfer. Vol. 39, No. 4, pp. 661–676, 1996
Elsevier Science Ltd
Printed in Great Britain

0017-9310(95)00174-3

Computation of permeability and dispersivities of solute or heat in periodic porous media

CHEO K. LEE, CHIN-CHENG SUN and CHIANG C. MEI†

Department of Civil and Environmental Engineering, Massachusetts Institute of Technology, Cambridge, MA 02139, U.S.A.

(*Received* 26 *August* 1994 *and in final form* 16 *May* 1995)

Abstract—We describe the numerical computations of permeability and dispersivities of solute and heat for a periodic porous medium by solving certain boundary value problems for a unit cell. These cell problems are derived from the asymptotic theory of homogenization which systematically accounts for the effects of micro(pore) scale mechanics on the macroscale processes. Variational principles are devised to replace the cell boundary value problems and are then used for finite-element computations. The geometry chosen consists of a cubic array of uniform grains of Wigner–Seitz shape. Comparisons of numerical results with available experimental data and with other theories are discussed.

INTRODUCTION

The dispersion of passive solute in porous media is of wide-ranging importance in environmental and chemical engineering, while the dispersion of heat is of interest to the study of geothermal energy exploration and underground disposal of nuclear wastes. In hydrology where geological complexities and uncertainties are unavoidable, it is customary to bypass the micromechanical details in the pores and to begin with the averaged law of Darcy for the flow and empirical relation for dispersion coefficients. From a more basic viewpoint the study of dispersion in porous media requires consideration of two important processes on the microscale. One is the fluid flow in the pores whose geometry is in general three-dimensional (3D) and complex. Another is the enhancement of diffusivity of solute or heat by the nonuniform convection in the pores. For both better scientific understanding of physics in disordered media and for direct applications to certain manufactured materials, theoretical investigations based on idealized models with an ordered micro-structure are helpful.

Many previous theories for flow-through 3D porous media are based on a periodic array of spheres. Hasimoto [1] obtained the periodic fundamental solution to the Stokes problem by Fourier series expansion, and applied the results analytically to a dilute array of uniform spheres. Sangani and Acrivos [2] extended the approximation [1] to calculate the drag force for higher concentration. Hasimoto's fundamental solution was also used in [3] to formulate an integral equation for the force distribution on an array of spheres for arbitrary concentration. By numerical solution of the integral equation, results for packed spheres were obtained for several porosity values. Continuous variation of porosity was examined only when the particles are in suspension. Strictly numerical computations have been made earlier based on series of trial functions and the Galerkin method for cubic packings of spheres in contact [4, 5]. A general theory of flow through periodic porous media has been advanced by Brenner (unpublished manuscripts cited in [6] and [7]) who showed how Darcy's law and the permeability tensor can in principle be computed from a cannonical boundary value problem in a unit cell.

Theories of dispersion in porous media began with analytical models where the pores are replaced by networks of tubes in which the flow velocity is assumed to be either uniform [8] or parabolic [9–11]; the 3D effects at junctions are ignored. For truly 3D grains and pores analytical theories are so far limited to dilute suspensions of spheres. By approximating the spheres as point forces, Koch and Brady [12] obtained some general results on the dependence of the longitudinal D_L and transverse D_T dispersivities on the local Peclet number Pe. The result shows good agreement with experimental data in [13]. For a periodic lattice of uniform spheres the direction of the mean flow is important [12]. If the flow is parallel to a lattice axis, $D_L \propto Pe^2$, but if the flow is inclined $D_L \propto Pe$ instead [14]. Koch *et al.* [14] further pointed out the qualitative differences between randomly distributed and cubically stacked spheres, at low concentration. For the latter geometry D_L is found to be nearly proportional to Pe^2. For a comprehensive survey the reader is referred to recent books [6, 15].

For arbitrary porosity and truly 3D grains and pores, a rigorous theoretical basis has been laid in [7] where the method of moments of Aris for tubular flows is extended to three dimensional flows in peri-

† Author to whom correspondence should be addressed.

NOMENCLATURE

A_s	surface area per grain
C	specific heat
D_L	longitudinal dispersivity
D_T	transverse dispersivity
$\mathbf{D}_{ij}$	symmetric dispersion tensor
$\bar{D}_{jm}$	normalized dispersivity
$\mathbf{E}_{ij}$	antisymmetric tensor
J	stationary functional
K	conductivity
k_{ij}	velocity in Stokes cell problem
$\langle k \rangle$	permeability
l	microscale, cell size
L	macroscale
M_m	fluid temperature in dispersion cell problem
N_m	solid temperature in dispersion cell problem
n	porosity
Pe	Peclet number
P_o	scale of pressure variation
Re	microscale Reynolds number
S_j	pressure in Stokes cell problem
t_1	convection time
t_2	diffusion time
U	scale of fluid velocity
$\langle u_i^{(u)} \rangle$	cell average of u_i^0
x_i	fast coordinate
X_i	slow coordinate
T_f, T_s	temperature
V_s	volume per grain.

Greek symbols

α_f	thermal diffusivity of fluid
δ_{ij}	Kronecker delta
ΔP	variation of
Δ	finite element mesh
Λ	Lagrange multiplier
μ	viscosity
Ω	unit micro cell
ρ	density
τ	time scale.

Superscripts

*	dimensional variables
(i)	ith order in perturbation.

Subscripts

f	fluid property
s	solid property
o	scale of dependent variables.

odic porous media. Brenner deduced the canonical boundary value problems in a unit cell, which must be solved to give first the interstitial flow and then dispersion tensor. Alternate theoretical arguments leading to the same canonical problems have been obtained by the method of local volume averaging [16], and by the asymptotic theory of homogenization [17–20]. Comprehensive surveys of these theories may be found in refs. [6, 15] and [21]. Numerical solution of these cell problems which are essential for obtaining quatitative information regarding the dispersion tensor is however not trivial. For body-centered cubic packing of spheres, Lee [22] was only successful in the limit of zero Peclet number Pe. For 2D periodic array of cylinders, the calculated D_L increases as $Pe^{1.7}$ and Pe^2 in [23] and [24], respectively, while D_T remains almost unchanged with Pe [24]. For 3D array of spheres, numerical results [25] also show D_L increasing as Pe^2, as predicted analytically in [14] for dilute spheres. Based on a theory employing the method of local volume averaging, numerical computation of heat dispersivities in 2D periodic array of cylinders has been performed in [26]. Unlike the results in refs. [23] and [24], the longitudinal dispersivity D_L increases as Pe^m where the exponent m varies from 1.71 to 1.86 for the in-line array and from 1.26 to 1.54 for the staggered array.

The purpose of this paper is to describe the numerical computation of permeability and dispersivities by solving the cell problems derived from the homogenization theory. On the microscale we consider a cubic array of uniform Wigner–Seitz grains [27] each of which is shaped like a cheap soccer ball [Fig. 1(a)]. Thus each cell is a cube containing just one grain surrounded by liquid. One advantage of this microcell geometry, unlike periodically packed spheres, is the wide range of continuously varying porosity from 1/6 to 5/6 for contacting grains. Details for solving two cell problems are described. The first cell problem is to find the Stokes' flow in a unit cell subject to unit global pressure gradient. The solution gives the local distributions of the pore fluid velocity from which the permeability is calculated. The second cell problem, called the B-field problem by Brenner, is for the convective diffusion inside the cell, whose solution gives the dispersivity for passive solute or heat. Both cell problems are solved by finite elements for which variational principles are first established. Numerical results for small to moderate Peclet numbers are presented and compared with existing theoretical and experimental data.

Before describing the computational effort, it is convenient to summarize the theoretical assumptions and framework regarding the fluid flow in the pores and the transport of heat (or solute) in the grains and in the pores.

FLOW IN THE PORES

Consider a model medium which is divisible into periodic cubes of dimension l. Let P_o be the charac-

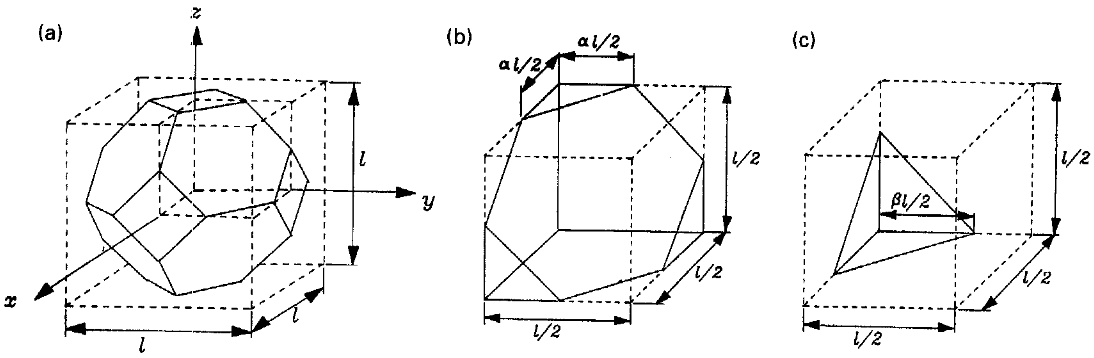

Fig. 1. (a) A microcell with a Wigner–Seitz grain, (b) 1/8-th of the Wigner–Seitz cell with grains in contact and (c) 1/8th of the Wigner–Seitz cell with grains in suspension.

teristic variation of global pressure P^* which may vary significantly (i.e. $\Delta P^*/P^* \leqslant O(1)$) over the global distance L. Thus the global pressure gradient is of the order $O(P_o/L)$. For generality we also allow the cell size to vary slowly over the global scale L in the sense that $\Delta l/l \leqslant O(1)$ over a distance L. Let the two length scales be in sharp contrast so that their ratio is a small parameter $\varepsilon = l/L \ll 1$. Limiting to creeping flows the local gradient must be comparable to the viscous stresses so that the local velocity is $U = O(P_o l^2/\mu L)$, where μ is the absolute viscosity of fluid. Denoting physical and dimensionless variables respectively by symbols with and without asterisks, the following normalization may be introduced in the Navier–Stokes equations

$$x_i^* = lx_i \quad \Delta P^* = P_o \Delta P \quad u_i^* = Uu_i \tag{1}$$

with $i = 1, 2, 3$. Two dimensionless parameters would then appear: the length ratio ε and the Reynolds number

$$Re = \frac{\rho U l}{\mu} = \frac{\rho P_0 l^2}{\mu^2} \frac{l}{L} \tag{2}$$

which will be assumed to be of order $O(\varepsilon)$. By introducing fast and slow variables, x_i and $X_i = \varepsilon x_i$, and multiple-scale expansions, it is then found that the leading order pore pressure $p^{(0)}$ depends only on the global scale, $p^{(0)} = p^{(0)}(X_i)$. By expressing the solution for $u_i^{(0)}, p^{(1)}$ in the following form

$$u_i^{(0)} = -k_{ij} \frac{\partial p^{(0)}}{\partial X_j} \tag{3a}$$

$$p^{(1)} = -S_j \frac{\partial p^{(0)}}{\partial X_j} + \bar{p}^{(1)} \tag{3b}$$

where $\bar{p}^{(1)}(X_i)$ depends on X_i only, the coefficients $k_{ij}(x_i, X_i)$ and $S_j(x_i, X_i)$ are found to be governed by the following canonical Stokes problem in the Ω cell:

$$\frac{\partial k_{ij}}{\partial x_i} = 0 \tag{4}$$

$$\frac{\partial S_j}{\partial x_i} - \nabla^2 k_{ij} = \delta_{ij} \tag{5}$$

in Ω_f, with

$$k_{ij} = 0 \quad \text{on} \quad \Gamma \tag{6}$$

$$k_{ij}, S_j \text{ are } \Omega\text{-periodic in } \Omega \text{ and on } \partial\Omega \tag{7}$$

where Γ and $\partial\Omega$ are respectively the fluid–solid interface and the boundary of the Ω-cell. Equations (4)–(7) constitute the first cell problem [28–32]. For a chosen granular geometry the numerical solution gives the local velocity and pressure fluctuation in terms of the global pressure gradient $\partial p^{(0)}/\partial X_j$. Let the volume average over a microcell be defined by

$$\langle f \rangle = \frac{1}{\Omega} \int_{\Omega_f} f \, \mathrm{d}\Omega \tag{8}$$

where Ω_f is the fluid volume in the cell. Then the average of equation (3a) gives the law of Darcy,

$$\langle u_i^{(0)} \rangle = -\langle \mathbf{k}_{ij} \rangle \frac{\partial p^{(0)}}{\partial X_j} \tag{9}$$

where $\langle \mathbf{k}_{ij} \rangle$ is the hydraulic conductivity tensor, which is the permeability tensor divided by μ.

For later use we note that in physical variables (marked by *), the symmetric hydraulic conductivity tensor is given by

$$\langle \mathbf{k}_{ij}^* \rangle = \langle \mathbf{k}_{ij} \rangle \frac{l^2}{\mu}. \tag{10}$$

CONVECTIVE DIFFUSION OVER MICRO- AND MACROSCALES

We shall summarize the results in [19, 20] obtained by applying the homogenization theory. Let the subscripts f and s distinguish quantities of the pore fluid and the solid grains, respectively. The starting basic equations for diffusion and convection of heat are given by

$$\rho_f C_f\left(\frac{\partial T_f}{\partial t}+u_j\frac{\partial T_f}{\partial x_j}\right)=K_f\frac{\partial^2 T_f}{\partial x_j\partial x_j}\quad x_k\in\Omega_f \tag{11}$$

$$\rho_s C_s\frac{\partial T_s}{\partial t}=K_s\frac{\partial^2 T_s}{\partial x_j\partial x_j}\quad x_k\in\Omega_s \tag{12}$$

where (T_f, T_s), (ρ_f, ρ_s), (K_f, K_s), (C_f, C_s) and (Ω_f, Ω_s) denote respectively the temperatures, densities, thermal conductivities, specific heats and partial volumes of the fluid and solid in the Ω cell. On the solid–fluid interface Γ, the temperatures and heat flux must be continuous:

$$T_f=T_s\quad x_k\in\Gamma \tag{13}$$

$$K_f\frac{\partial T_f}{\partial x_k}n_k=K_s\frac{\partial T_s}{\partial x_k}n_k\quad x_k\in\Gamma \tag{14}$$

where n_k represents the components of the unit normal vector pointing out of the fluid. In equations (11) and (12), energy dissipation by viscous stresses has been neglected, which is justifiable for low Reynolds number flows. The transport of passive solute is a special case with $K_s\equiv 0$.

Let us distinguish the cell-averages of quantities in the pore fluid and in the solid grains by

$$\langle F_f\rangle=\frac{1}{\Omega}\iiint_{\Omega_f}F_f\,d\Omega_f\quad \langle F_s\rangle=\frac{1}{\Omega}\iiint_{\Omega_s}F_s\,d\Omega_s \tag{15}$$

where Ω_f, Ω_s and Ω are respectively the volume of the pore fluid, the solid matrix and the total composite in the unit cell. To get the effective convection–diffusion equation, one needs to solve the following two canonical cell problems for the two vectors $\{M_m\}$ and $\{N_m\}$:

$$\rho_f C_f u_j^{(0)}\frac{\partial M_m}{\partial x_j}-K_f\frac{\partial^2 M_m}{\partial x_j\partial x_j}=\rho_f C_f\tilde{u}_m^{(0)}\quad x_i\in\Omega_f \tag{16}$$

$$K_s\frac{\partial^2 N_m}{\partial x_j\partial x_j}=\rho_s C_s\frac{\rho_f C_f}{\langle\rho C\rangle}\langle u_m^{(0)}\rangle\quad x_i\in\Omega_s \tag{17}$$

where n denotes the porosity and

$$\langle\rho C\rangle=n\rho_f C_f+(1-n)\rho_s C_s \tag{18}$$

is the Ω-cell average of ρC and $\langle u_j^{(0)}\rangle$ in dimensionless form has been given in equation (9). In addition, $\tilde{u}_j^{(0)}$ denotes the following difference,

$$\tilde{u}_j^{(0)}=u_j^{(0)}-\frac{\rho_f C_f}{\langle\rho C\rangle}\langle u_j^{(0)}\rangle \tag{19}$$

with the boundary conditions

$$M_m=N_m\quad x_j\in\Gamma \tag{20}$$

$$\left(K_f\frac{\partial M_m}{\partial x_j}-K_s\frac{\partial N_m}{\partial x_j}\right)n_j=(K_f-K_s)n_m\quad x_j\in\Gamma \tag{21}$$

and Ω periodicity. To render the solution unique we further require that

$$\langle M_m\rangle=\langle N_m\rangle=0. \tag{22}$$

After these vectors are solved numerically for a given cell geometry, an effective convective–diffusion equation on the macroscale can be derived [19, 20]. In particular, the dispersion tensor due to interstitial shear is defined in terms of M_j, N_j according to

$$D_{jm}=K_f\left[\left\langle\frac{\partial M_j}{\partial x_k}\frac{\partial M_m}{\partial x_k}\right\rangle-\left\langle\frac{\partial M_m}{\partial x_j}+\frac{\partial M_j}{\partial x_m}\right\rangle\right]+K_s\left[\left\langle\frac{\partial N_j}{\partial x_k}\frac{\partial N_m}{\partial x_k}\right\rangle-\left\langle\frac{\partial N_m}{\partial x_j}+\frac{\partial N_j}{\partial x_m}\right\rangle\right]. \tag{23}$$

For a nonconducting solid matrix or for a passive solute, $K_s=0$, (23) reduces to the result in refs. [7] and [32] exactly. Since M_m and N_m depend on K_f and K_s nonlinearly, as is evident from the Ω cell problem defining them in Section 3, D_{jm} does not necessarily vanish as K_f and K_s approach zero. This is known for the special case of solute dispersion in a porous matrix composed of parallel tubes [7, 32].

Numerical results will be presented as functions of Peclet numbers, defined separately for heat and for passive solute as follows

$$Pe=\frac{\rho_f C_f Ul}{K_f}\text{(heat)}\quad Pe=\frac{Ul}{\kappa}\text{(solute)} \tag{24}$$

where $\kappa=K_f/(\rho_f C_f)$ is the molecular diffusivity of solute. U is the average of fluid velocity over the entire cell volume including the solid phase. For solute only, the dimensionless total dispersivity is found from equation (23) by omitting the solid phase,

$$\bar{D}_{jm}=\frac{\langle K\rangle+D_{jm}}{\langle\rho C\rangle\kappa}=\frac{\langle K\rangle+D_{jm}}{n\rho_f C_f\kappa}=1+\frac{1}{n}\left[\left\langle\frac{\partial M_j}{\partial x_k}\frac{\partial M_m}{\partial x_k}\right\rangle-\left\langle\frac{\partial M_m}{\partial x_j}+\frac{\partial M_j}{\partial x_m}\right\rangle\right] \tag{25}$$

since $K_f/(\rho_f C_f)=\kappa$. The right-hand side of (25) is the volume average over Ω_f only. For heat transport the dimensionless total dispersivity is defined as follows.

$$\bar{D}_{jm}=\frac{\langle K\rangle+D_{jm}}{\langle\rho C\rangle}\bigg/\frac{K_f}{(\rho_f C_f)}=\left\{\frac{\langle K\rangle}{K_f}+\left[\left\langle\frac{\partial M_j}{\partial x_k}\frac{\partial M_m}{\partial x_k}\right\rangle-\left\langle\frac{\partial M_m}{\partial x_j}+\frac{\partial M_j}{\partial x_m}\right\rangle\right]+\frac{K_s}{K_f}\left[\left\langle\frac{\partial N_j}{\partial x_k}\frac{\partial N_m}{\partial x_k}\right\rangle-\left\langle\frac{\partial N_m}{\partial x_j}+\frac{\partial N_j}{\partial x_m}\right\rangle\right]\right\}\bigg/\left(n+\frac{\rho_s C_s}{\rho_f C_f}(1-n)\right). \tag{26}$$

UNIQUENESS OF THE CELL PROBLEM

Suppose that $\tilde{M}_m$ and $\tilde{N}_m$ represent the difference of two solutions of the inhomogeneous problems (16)–(22), the vector quantities $\tilde{M}_m$ and $\tilde{N}_m$ must satisfy the homogeneous equations

$$\rho_f C_f u_j^{(0)} \frac{\partial \tilde{M}_m}{\partial x_j} - K_f \frac{\partial^2 \tilde{M}_m}{\partial x_j \partial x_j} = 0 \quad x_i \in \Omega_f \tag{27}$$

$$K_s \frac{\partial^2 \tilde{N}_m}{\partial x_j \partial x_j} = 0 \quad x_i \in \Omega_s \tag{28}$$

$$\tilde{M}_m = \tilde{N}_m \quad x_i \in \Gamma \tag{29}$$

$$K_f \frac{\partial \tilde{M}_m}{\partial x_j} n_j = K_s \frac{\partial \tilde{N}_m}{\partial x_j} n_j \quad x_i \in \Gamma \tag{30}$$

$$\tilde{M}_m \quad \text{and} \quad \tilde{N}_m \text{ are } \Omega\text{-periodic} \tag{31}$$

$$\langle \tilde{M}_m \rangle = \langle \tilde{N}_m \rangle = 0. \tag{32}$$

Multiplying (27) by $\tilde{M}_m$ and (28) by $\tilde{N}_m$ and integrating over Ω_f and Ω_s, we obtain after using Gauss's theorem, Ω-periodicity and the boundary conditions (29) and (30), that

$$\int_{\Omega_f} K_f \frac{\partial \tilde{M}_m}{\partial x_j} \frac{\partial \tilde{M}_m}{\partial x_j} \mathrm{d}\Omega + \int_{\Omega_s} K_s \frac{\partial \tilde{N}_m}{\partial x_j} \frac{\partial \tilde{N}_m}{\partial x_j} \mathrm{d}\Omega = 0. \tag{33}$$

For the left-hand side to vanish, the thermal gradients $\partial \tilde{M}_m/\partial x_j$ and $\partial \tilde{N}_m/\partial x_j$ must be zero. Then $\tilde{M}_m$ and $\tilde{N}_m$ can at most be microscale-independent constants. Let these constants be C_1 and C_2, respectively in Ω_f and Ω_s. Equations (29) and (32) guarantee that $C_1 = C_2 = 0$, hence

$$\tilde{M}_m = \tilde{N}_m = 0 \tag{34}$$

and the cell problem has a unique solution.

Instead of the constraint (22) to ensure uniqueness, we have tried (as in refs. [26] and [33]) at first the apparent alternative by assigning a fixed value for either M_m or N_m at an arbitrarily chosen point in the unit cell. The rationale is that solutions corresponding to different choice of points would differ at most by a constant which would not affect the dispersivity. It will now be shown that this alternative does not ensure uniqueness and hence is unsatisfactory theoretically. Let (M_m, N_m) and (M'_m, N'_m) be two solutions satisfying equations (16)–(21), and obeying the following constraint at different points in Ω_f, $M_m(P) = 0$ and $M'_m(P') = 0$. Let us assume that the two solutions differ only by a microscale-independent constant, then their differences $\tilde{M}_m = M_m - M'_m$ and $\tilde{N}_m = N_m - N'_m$ should be uniform in the microcell. These differences must satisfy equations (27)–(31) and the following conditions

$$\tilde{M}_m(P) = -M'_m(P) \quad \text{and} \quad \tilde{M}_m(P') = M_m(P').$$

It follows from (33) that either $\tilde{M}_m = -M'_m(P)$ or $\tilde{M}_m = M_m(P')$. But $-M'_m(P)$ and $M_m(P')$ are in general not identical, hence $\tilde{M}_m$ cannot be constant, and the original assumption is false.

The numerical method of finite elements will be used to solve the cell boundary value problems for the Stokes flow defined earlier, and for the convective diffusion of solute or heat defined above. To ensure that the matrices for the nodal coefficients are symmetric, we first replace the cell problems by variational principles; this reduces computer storage and enhances numerical efficiency.

VARIATIONAL PRINCIPLE FOR STOKES PROBLEM IN A CELL

By standard arguments it is possible to derive from the governing equations of the Stokes problem that

$$\delta J = 0 \tag{35}$$

where J is

$$J = \frac{1}{2} \int_{\Omega_f} \frac{\partial k_{ij}}{\partial x_m} \frac{\partial k_{ij}}{\partial x_m} \mathrm{d}\Omega + \int_{\Omega_f} k_{ij} \left(\frac{\partial S_j}{\partial x_i} - \delta_{ij} \right) \mathrm{d}\Omega. \tag{36}$$

We find it convenient to verify (35) by taking the first variation of (36) and by integration by parts

$$\begin{aligned}
\delta J &= \int_{\Omega_f} \frac{\partial k_{ij}}{\partial x_m} \frac{\partial \delta k_{ij}}{\partial x_m} \mathrm{d}\Omega + \int_{\Omega_f} \delta k_{ij} \left(\frac{\partial S_j}{\partial x_i} - \delta_{ij} \right) \mathrm{d}\Omega \\
&\quad + \int_{\Omega_f} k_{ij} \frac{\partial \delta S_j}{\partial x_i} \mathrm{d}\Omega \\
&= \oint_{\partial\Omega_f} \delta k_{ij} \frac{\partial k_{ij}}{\partial x_m} n_m \,\mathrm{d}S - \int_{\Omega_f} \delta k_{ij} \frac{\partial^2 k_{ij}}{\partial x_m \partial x_m} \mathrm{d}\Omega \\
&\quad + \int_{\Omega_f} \delta k_{ij} \left(\frac{\partial S_j}{\partial x_i} - \delta_{ij} \right) \mathrm{d}\Omega \\
&\quad + \oint_{\partial\Omega_f} k_{ij} \delta S_j n_i \,\mathrm{d}S - \int_{\Omega_f} \frac{\partial k_{ij}}{\partial x_i} \delta S_j \,\mathrm{d}\Omega \\
&= \oint_{\partial\Omega_f} \delta k_{ij} \frac{\partial k_{ij}}{\partial x_m} n_m \,\mathrm{d}S + \oint_{\partial\Omega_f} \delta S_j k_{ij} n_i \,\mathrm{d}S \\
&\quad + \int_{\Omega_f} \delta k_{ij} \left(\frac{\partial S_j}{\partial x_i} - \frac{\partial^2 k_{ij}}{\partial x_m \partial x_m} - \delta_{ij} \right) \mathrm{d}\Omega \\
&\quad - \int_{\Omega_f} \delta S_j \frac{\partial k_{ij}}{\partial x_i} \mathrm{d}\Omega.
\end{aligned}$$

Here $\partial\Omega$ and $\partial\Omega_f$ denote respectively the boundaries of the cell and of the fluid phase in the cell. In the unit cell, the fluid surface $\partial\Omega_f$ consists of two parts: the fluid–solid interface Γ, and the fluid part of the cell boundary $\partial\Omega_f \cap \partial\Omega$. Now the volume integrals above vanish because of equations (4) and (5), while the surface integrals vanish because of (6) and (7). The reverse is also true. Hence the cannonical Stokes problem in the Ω cell is the same as (35).

VARIATIONAL PRINCIPLE FOR CONVECTIVE DIFFUSION IN A CELL

Since the pore fluid velocity is already known by solving the Stokes cell problem, we have $\delta u_j^{(0)} = 0$.

The variations δM_m and δN_m must satisfy the homogeneous equations (27)–(32).

To derive the variational principle, we first multiply (16) by δM_m and (17) by δN_m, and integrate over the respective phase. Similarly, we replace $\tilde{M}_m$ by δM_m and $\tilde{N}_m$ by δN_m in equations (27)–(31), multiply the resulting (27) by M_m and (28) by N_m, and then integrate the sum of these products over the respective phases. The results are then added and conditions on the interface and Ω-periodicity are applied. If the constraint (22) is further incorporated by the Lagrange multiplier method, a variational principle equivalent to (16) to (22) can be obtained so that

$$\delta J = 0 \tag{37}$$

where the functional J is

$$\begin{aligned} J = & \int_{\Omega_f} \left(-\rho_f C_f \tilde{u}_m^{(0)} M_m + \rho_f C_f u_j^{(0)} M_m \frac{\partial M_m}{\partial x_j} \right. \\ & \left. + K_f \frac{\partial M_m}{\partial x_j} \frac{\partial M_m}{\partial x_j} - K_f \frac{\partial M_m}{\partial x_m} \right) \mathrm{d}\Omega \\ & + \int_{\Omega_s} \left(\frac{(\rho_s C_s)(\rho_f C_f)}{\langle \rho C \rangle} \langle u_j^{(0)} \rangle N_m \right. \\ & \left. + K_s \frac{\partial N_m}{\partial x_j} \frac{\partial N_m}{\partial x_j} - K_s \frac{\partial N_m}{\partial x_m} \right) \mathrm{d}\Omega \\ & + \lambda_m \left(\int_{\Omega_f} M_m \,\mathrm{d}\Omega + \int_{\Omega_s} N_m \,\mathrm{d}\Omega \right) \end{aligned} \tag{38}$$

in which λ_m is the Lagrange multiplier. In the case of passive solute, one simply omits the solid part in equation (38).

For brevity we only verify that the set of conditions (16)–(22), indeed, extremizes the functional J. By taking the first variation of J we get

$$\begin{aligned} \delta J = & \int_{\Omega_f} \left(-\rho_f C_f \tilde{u}_m^{(0)} + \rho_f C_f u_j^{(0)} \frac{\partial M_m}{\partial x_j} \right) (\delta M_m) \,\mathrm{d}\Omega \\ & + \int_{\Omega_f} \left[\rho_f C_f u_j^{(0)} \frac{\partial (\delta M_m)}{\partial x_j} M_m \right. \\ & \left. + 2K_f \frac{\partial M_m}{\partial x_j} \delta \left(\frac{\partial M_m}{\partial x_j} \right) - K_f \frac{\partial (\delta M_m)}{\partial x_m} \right] \mathrm{d}\Omega \\ & + \int_{\Omega_s} \left[2K_s \frac{\partial N_m}{\partial x_j} \delta \left(\frac{\partial N_m}{\partial x_j} \right) \right. \\ & \left. - K_s \frac{\partial (\delta N_m)}{\partial x_m} + \frac{(\rho_s C_s)(\rho_f C_f)}{\langle \rho C \rangle} \langle u_j^{(0)} \rangle \delta N_m \right] \mathrm{d}\Omega \\ & + \left(\int_{\Omega_f} M_m \,\mathrm{d}\Omega + \int_{\Omega_s} N_m \,\mathrm{d}\Omega \right) \delta \lambda_m \\ & + \lambda_m \delta \left(\int_{\Omega_f} M_m \,\mathrm{d}\Omega + \int_{\Omega_s} N_m \,\mathrm{d}\Omega \right). \end{aligned} \tag{39}$$

After using equation (27), the integrand of the second integral in Ω_f can be further written,

$$\begin{aligned} & \rho_f C_f u_j^{(0)} \frac{\partial (\delta M_m)}{\partial x_j} M_m + 2K_f \frac{\partial M_m}{\partial x_j} \delta \left(\frac{\partial M_m}{\partial x_j} \right) - K_f \frac{\partial (\delta M_m)}{\partial x_m} \\ & = K_f M_m \frac{\partial^2 (\delta M_m)}{\partial x_j \partial x_j} + 2K_f \frac{\partial M_m}{\partial x_j} \delta \left(\frac{\partial M_m}{\partial x_j} \right) - K_f \frac{\partial (\delta M_m)}{\partial x_m} \\ & = K_f \frac{\partial}{\partial x_j} \left(M_m \frac{\partial (\delta M_m)}{\partial x_j} \right) + K_f \frac{\partial}{\partial x_j} \left(\frac{\partial M_m}{\partial x_j} (\delta M_m) \right) \\ & \quad - K_f \frac{\partial^2 M_m}{\partial x_j \partial x_j} (\delta M_m) - K_f \frac{\partial (\delta M_m)}{\partial x_m}. \end{aligned} \tag{40}$$

Similarly, the integrand of the third integral, except the last term, becomes

$$\begin{aligned} & 2K_s \frac{\partial N_m}{\partial x_j} \delta \left(\frac{\partial N_m}{\partial x_j} \right) - K_s \frac{\partial (\delta N_m)}{\partial x_m} \\ & = K_s \frac{\partial}{\partial x_j} \left(\frac{\partial N_m}{\partial x_j} \delta N_m \right) - K_s \frac{\partial^2 N_m}{\partial x_j \partial x_j} (\delta N_m) \\ & \quad + K_s \frac{\partial}{\partial x_j} \left(N_m \frac{\partial (\delta N_m)}{\partial x_j} \right) \\ & \quad - K_s N_m \frac{\partial^2 (\delta N_m)}{\partial x_j \partial x_j} - K_s \frac{\partial (\delta N_m)}{\partial x_m} \\ & = -K_s \frac{\partial^2 N_m}{\partial x_j \partial x_j} (\delta N_m) + K_s \frac{\partial}{\partial x_j} \\ & \quad \times \left(\frac{\partial N_m}{\partial x_j} \delta N_m + N_m \frac{\partial (\delta N_m)}{\partial x_j} \right) - K_s \frac{\partial (\delta N_m)}{\partial x_m} \end{aligned} \tag{41}$$

where (28) has been used.

Substituting equations (40) and (41) into (39) and making use of Gauss's theorem, we obtain

$$\begin{aligned} \delta J = & \int_{\Omega_f} \left(-\rho_f C_f \tilde{u}_m^{(0)} + \rho_f C_f u_j^{(0)} \frac{\partial M_m}{\partial x_j} \right. \\ & \left. - K_f \frac{\partial^2 M_m}{\partial x_j \partial x_j} \right) (\delta M_m) \,\mathrm{d}\Omega \\ & + \int_{\Omega_s} \left(\frac{(\rho_s C_s)(\rho_f C_f)}{\langle \rho C \rangle} \langle u_j^{(0)} \rangle - K_s \frac{\partial^2 N_m}{\partial x_j \partial x_j} \right) (\delta N_m) \,\mathrm{d}\Omega \\ & + \int_{\Gamma} \left[K_f M_m \frac{\partial (\delta M_m)}{\partial x_j} - K_s N_m \frac{\partial (\delta N_m)}{\partial x_j} \right] n_j \,\mathrm{dS} \\ & + \int_{\Gamma} \left[\left(K_f \frac{\partial M_m}{\partial x_j} n_j - n_m \right) (\delta M_m) \right. \\ & \left. - \left(K_s \frac{\partial N_m}{\partial x_i} n_j - n_m \right) (\delta N_m) \right] \mathrm{dS} \\ & + \int_{\Gamma_f} \left\{ K_f \left[M_m \frac{\partial (\delta M_m)}{\partial x_j} \right. \right. \\ & \left. \left. + \frac{\partial M_m}{\partial x_j} (\delta M_m) \right] n_j - K_f (\delta M_m) n_m \right\} \mathrm{dS} \\ & - \int_{\Gamma_s} \left\{ K_s \left[N_m \frac{\partial (\delta N_m)}{\partial x_j} \right. \right. \end{aligned}$$

$$+\frac{\partial N_m}{\partial x_j}(\delta N_m)\Big]n_j - K_s(\delta N_m)n_m\Big\}\,dS$$

$$+\left(\int_{\Omega_f} M_m\,d\Omega + \int_{\Omega_s} N_m\,d\Omega\right)\delta\lambda_m$$

$$+\lambda_m\delta\left(\int_{\Omega_f} M_m\,d\Omega + \int_{\Omega_s} N_m\,d\Omega\right)$$

where Γ_f and Γ_s are respectively the fluid and solid portions of the surface of the cubic microcell. The shapes of Γ_f and Γ_s are the same on opposite faces of the cell due to Ω-periodicity.

For arbitrary δM_m and δN_m, the surface integrals on the interface Γ vanish because of the boundary conditions. The integral over Γ_f is also zero due to Ω-periodicity and the fact that n_j is of opposite sign on Γ_f. Similarly the integral over Γ_s vanishes. Condition (22) implies the same for the last two integrals. Finally the first two volume integrals vanish on account of the two governing equations (16) and (17). Thus equations (16)–(22) imply equation (37). The reverse can also be shown by the standard argument of contradiction. Thus $\delta J = 0$ is equivalent to the boundary value problems (10)–(22).

PROPERTIES OF THE WIGNER–SEITZ GRAIN

For a model microcell geometry of periodic porous medium we choose the Wigner–Seitz grain shown in Fig. 1(a).

Referring to Fig. 1(a) and (b), we let l be one side of the unit cube containing one grain, and αl be the diagonal length of the solid part on the upper and lower boundaries of the cell. It can be shown by elementary geometry that the solid volume is

$$V_s = \left[\tfrac{1}{6}(1+\alpha)^3 - \frac{\alpha^3}{2}\right]l^3 \tag{42}$$

and the surface area of the grain is

$$A_s = \sqrt{3}(1+2\alpha-2\alpha^2)l^2 + 3\alpha^2 l^2. \tag{43}$$

The porosity is therefore

$$n = 1 - \left[\tfrac{1}{6}(1+\alpha)^3 - \frac{\alpha^3}{2}\right]. \tag{44}$$

For later use we define the shape parameter by

$$\frac{V_s}{A_s l} = \frac{\left[\tfrac{1}{6}(1+\alpha)^3 - \dfrac{\alpha^3}{2}\right]}{\sqrt{3}(1+2\alpha-2\alpha^2)+3\alpha^2} \tag{45}$$

which is uniquely related to n–α. For $\alpha = 0$ the grain is shaped as a diamond with $n = 5/6 = 0.8333$ [Fig. 1(b)]. For $\alpha = 1$, i.e. $n = 1/6 = 0.1667$, fluid is trapped and cannot flow from one pore to another. Thus for cubic packing of contacting Wigner–Seitz grains the porosity varies continuously between 1/6 and 5/6 for $1 > \alpha > 0$. We have also performed computations for porosities larger than 0.8333, corresponding to grains fixed in space but not in contact [Fig. 1(c)]. The solid volume and surface area of a diamond are then $V_s = \beta^3 l^3/6$ and $A_s = \sqrt{3}\beta^2 l^2$, respectively, where β is defined to be the ratio of the total height of the diamond to the cell height as shown in Fig. 1(c).

FINITE-ELEMENT APPROXIMATION

The plane boundaries of the Wigner–Seitz grain are particularly suited for finite elements.

For the Stokes cell problem, we assume that

$$k_{ij} = \sum_l k_{ij}^{(l)} N^{(l)} \qquad S_j = \sum_m S_j^{(m)} M^{(m)} \tag{46}$$

where $N^{(l)}$, $M^{(m)}$ are shape functions for k_{ij} and S_j in elements (l) and (m), respectively, and $k_{ij}^{(l)}, S_j^{(m)}$ are the unknown nodal coefficients for k_{ij} and S_j in each element. Substituting (46) into (36), and equating to zero the derivatives of J with respect to $k_{ij}^{(n)}$ and then with respect to $S_j^{(m)}$, we have

$$\frac{\partial J}{\partial k_{ij}^{(n)}} = \int_{\Omega_f} \frac{\partial N^{(n)}}{\partial x_m}\sum_l \frac{\partial N^{(l)}}{\partial x_m} k_{ij}^{(l)}\,d\Omega + \int_{\Omega_f} N^{(n)}\left(\sum_m S_j^{(m)}\frac{\partial M^{(m)}}{\partial x_i} - \delta_{ij}\right)d\Omega = 0 \tag{47}$$

$$\frac{\partial J}{\partial S_j^{(m)}} = \int_{\Omega_f}\left(\sum_l k_{ij}^{(l)} N^{(l)}\right)\frac{\partial M^{(m)}}{\partial x_i}\,d\Omega = 0. \tag{48}$$

Equations (47) and (48) form a system of coupled matrix equations for $k_{ij}^{(l)}$ and $S_j^{(m)}$. The global matrix system is symmetric and is of the form:

$$\begin{bmatrix} A & 0 & 0 & B \\ 0 & A & 0 & C \\ 0 & 0 & A & D \\ B & C & D & 0 \end{bmatrix}\begin{Bmatrix} k_{1j}^{(l)} \\ k_{2j}^{(l)} \\ k_{3j}^{(l)} \\ S_j^{(m)} \end{Bmatrix} = \begin{Bmatrix} \int N^{(n)}\delta_{1j}\,d\Omega \\ \int N^{(n)}\delta_{2j}\,d\Omega \\ \int N^{(n)}\delta_{3j}\,d\Omega \\ 0 \end{Bmatrix} \tag{49}$$

where A, B, C, D have the following matrix elements:

$$A_{nl} = \int \frac{\partial N^{(n)}}{\partial x_j}\frac{\partial N^{(l)}}{\partial x_j}\,d\Omega$$

$$B_{nm} = \int N^{(n)}\frac{\partial M^{(m)}}{\partial x_1}\,d\Omega$$

$$C_{nm} = \int N^{(n)}\frac{\partial M^{(m)}}{\partial x_2}\,d\Omega$$

$$D_{nm} = \int N^{(n)} \frac{\partial M^{(m)}}{\partial x_3} \mathrm{d}\Omega. \tag{50}$$

The symmetry of the stiffness matrix in (49) enhances computational economy.

Because of the symmetry of the permeability tensor, $\langle \mathbf{k}_{ij} \rangle = \langle \mathbf{k}_{ji} \rangle$ and the symmetry of the grain geometry, only three coefficients among nine of $\langle \mathbf{k}_{ij} \rangle$ need to be computed, e.g. $\langle k_{11} \rangle (= \langle k_{22} \rangle = \langle k_{33} \rangle)$, $\langle k_{21} \rangle$ $(= \langle k_{12} \rangle)$ and $\langle k_{23} \rangle (= \langle k_{32} \rangle)$. Only one component, say S_1, is needed. Also, only 1/8 of the unit cell is needed for computation [Fig. 1(b) and (c)]. In the finite element calculations, quadratic tetrahedral elements are chosen for $N^{(l)}$ and linear tetrahedral elements for $M^{(m)}$. The frontal method [34] is used to solve the coupled matrix equation.

The finite-element approximation of the convective diffusion problem in a cell is treated similarly. Linear tetrahedral elements are used to represent the unknowns M_m and N_m. The first variation with respect to the unknown nodal coefficients and the unknown Lagrange multiplier is then taken to obtain algebraic equations for these unknowns. The straightforward details are omitted here.

NUMERICAL RESULTS FOR PERMEABILITY

Computations have been performed for contacting grains $\alpha = 0.85 \sim 0.0$ corresponding to porosities $n = 0.2518 \sim 0.8333$, and for fixed but non-contacting grains ($\beta = 0.9 \sim 0.5$ corresponding to $n = 0.8785 \sim 0.9792$). The length ratios α and β have been defined in Fig. 1(b) and (c). For $(\partial p^{(0)}/\partial X) = 1$, the local distributions of k_{ij} and S_j are first obtained; the results are then used to compute the permeability. We have checked that $\langle k_{11} \rangle \neq 0$, and all other components vanish: $\langle k_{21} \rangle = \langle k_{31} \rangle = \langle S_1 \rangle = 0$, as expected from symmetry. Five different meshes are used, with the number of nodes in 1/8 of the cell being 363, 2309, 7183, 16329 and 31091. By polynomial extrapolation, we get the final results for zero mesh size. Calculations are done on DEC Station 5000 and Cray XMP.

The hydraulic conductivity has been measured in the laboratory for different granular materials and porosity ($0.35 < n < 0.66$), based on which the following empirical Kozeny–Carman formula is well known [35, 36],

$$\langle k \rangle = \frac{1}{5} \frac{n^3}{(1-n)^2} \left(\frac{V_s}{A_s l} \right)^2 . \tag{51}$$

The materials examined for this formula include manufactured grains such as glass spheres (0.025 cm $\sim$ 0.1025 cm diameter), hexagonal prisms (0.48 cm length and 0.47 cm diameter), cubes (0.56 cm) as well as sand and powder. A large part of the data is for nearly uniform spheres with porosity close or equal to 0.39. It should be noted that, while the Kozeny–Carman formula is a best fit to experimental data for all grain shapes, data scatter lies between 10 and 20% due likely to the nonuniformity of sizes and the irregularity in shapes of sand particles.

In Fig. 2(a), the theoretical values of $\langle k_{11} \rangle$ for the Wigner–Seitz grain are compared with the empirical formula (51), for which the shape factor is given by (45). Within the range $0.37 < n < 0.68$ for which the empirical formula is based on experiments, our results are consistent and in trend with, but fall slightly below, the empirical formula. Outside this range of porosities, the deviation increases; but equation (51) itself is an extrapolation of measured data and may not be totally accurate.

In Fig. 2(b), our results are compared to numerical values by Zick and Homsy [3] for uniform spheres of various packings. They calculated the drag coefficient for a single sphere in an infinite array normalized by the Stokes drag formula for a sphere in an infinite fluid. The permeability for cubic packings of spheres shown in Fig. 3 have been converted from the drag force results of [3]. As mentioned before, for porosity greater than the minimum in each packing, i.e. $n = 0.48, 0.32, 0.26$ for simple cubic(SC), body-centered cubic(BCC), face-centered cubic(FCC), respectively, the spheres are not in contact. Discrepancies between the packed spheres and the Wigner–Seitz grains are expected to be the greatest for close packing, since particle interaction is affected by the geometry most significantly. This is indeed shown in Fig. 2(b) for low porosity. At higher porosity, the two theories agree remarkably well.

The local variation of k_{ij}, which will be used for the calculation of the dispersivity tensor, is not described here.

COMPUTATIONAL ASPECTS FOR CONVECTIVE DIFFUSION IN A CELL

By solving for M_m and N_m and then calculating the volume averages of their derivatives as defined in equations (25) and (26), numerical results for the dispersivities are obtained for two porosities: 0.38 and 0.5. The mean flow is assumed to be directed along the positive x-axis ($\theta = 0°$). By virtue of symmetry about the plane $z = 0$, the computational domain is then reduced to one half of the Wigner–Seitz cell in the region $-0.5 < x < 0.5$, $-0.5 < y < 0.5$ and $0 < z < 0.5$. Four meshes are used with the total number of nodes in 1/2 cell being 3610, 8125, 15376 and 26011. For all but the largest Pe polynomial extrapolation is used to get the dispersivities corresponding to zero mesh. As a measure of convergence with decreasing mesh size and accuracy of extrapolation, an error is defined by

$$\delta(\Delta) = \frac{\bar{D}_{jm}(\Delta) - \bar{D}_{jm}(0)}{\bar{D}_{jm}(\Delta)} \tag{52}$$

where $\bar{D}_{jm}(\Delta)$ is the dispersivity calculated for the finest mesh and $\bar{D}_{jm}(0)$ is the extrapolated value for zero mesh. The extrapolation error ranges from 0.475%

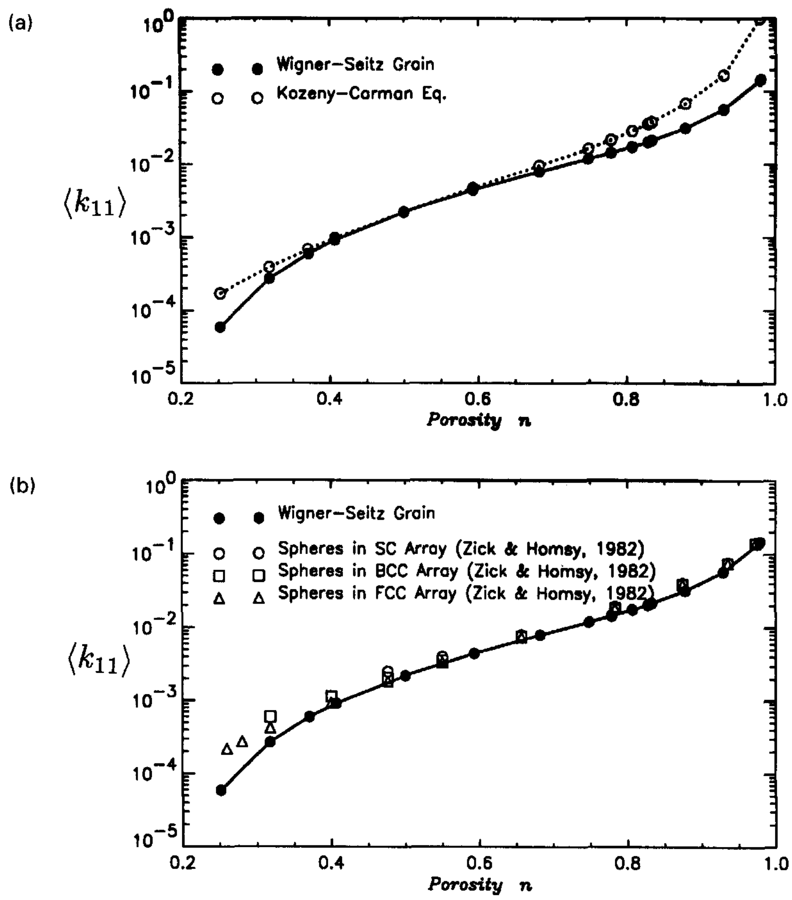

Fig. 2. The permeability $\langle k_{11} \rangle$ for the Wigner–Seitz grain: (a) comparison with the empirical Kozeny–Carman formula and (b) comparison with Zick and Homsy (1982)'s results for periodic array of spheres.

for $Pe = 0.1$ to 2.91% for $Pe = 200$. For the largest Pe (passive solute: 300 for D_L and 200 for D_T, and heat: 300 for both D_L and D_l), the results are obtained only by using the finest mesh. Computations for still higher Pe yielded errors larger than a few percent and are not reliable.

COMPUTED DISPERSIVITY FOR PASSIVE SOLUTE

In the models of a random network of capillaries [8–10], or randomly distributed dilute spheres [12] the dispersion coefficients are independent of the direction of mean flow. Because of the crystalline structure of the cubic array, our dispersivity tensor depends, however, on the direction of the global flow. In all our computations the mean flow is directed along the x axis ($\theta = 0°$). $\mathbf{D}_{ij}$ is diagonal with two independent components which are the longitudinal D_L and transverse D_T diffusivities: $D_{11}(\theta = 0) = D_L$ and $D_{22}(\theta = 0) = D_{33}(\theta = 0) = D_T$. For any other flow direction in the xy-plane, there are four non-zero independent dispersivity coefficients: D_{11}, D_{22}, D_{33} and $D_{12} = D_{21}$ by symmetry and $D_{13} = D_{23} = 0$.

Computed values of longitudinal and transverse dispersivity coefficients D_L and D_T are shown in Fig. 3(a) and (b), respectively for Pe up to 300 for D_L and 200 for D_T, for two porosities $n = 0.38$ and 0.5. To conform with experimental literature the abscissas in Fig. 3(a) and (b) are the Peclet numbers defined in terms of the mean flow velocity averaged over Ω_f only, i.e. $\langle u \rangle l/nD = Pe/n$. In Fig. 3(a), the longitudinal dispersivity is also compared with the measured data [37] for simple cubic packing of uniform spheres and the calculations [25] for a simple cubic lattice of uniform spheres with $n = 0.48$, 0.74 and 0.82. The results for $n = 0.48$ by Koch *et al.* [14] based on an approximate analysis for dilute concentration are also included. All are in qualitative agreement for D_L.

From the numerical results for $n = 0.38$ and 0.5, we see that for small Pe where molecular diffusion is dominant, the effective diffusivity defined in (43) is greater for the larger porosity. The reason is that the cross-sectional area through which a passive solute can diffuse increases with porosity. It is always less than unity in the diffusion-dominated regime since the presence of solid grains reduces the diffusive flux of solute. At the limit of $Pe = 0$, the effective diffusivity should be close to the effective thermal conductivity for closely packed spheres. For a closely packed cubic

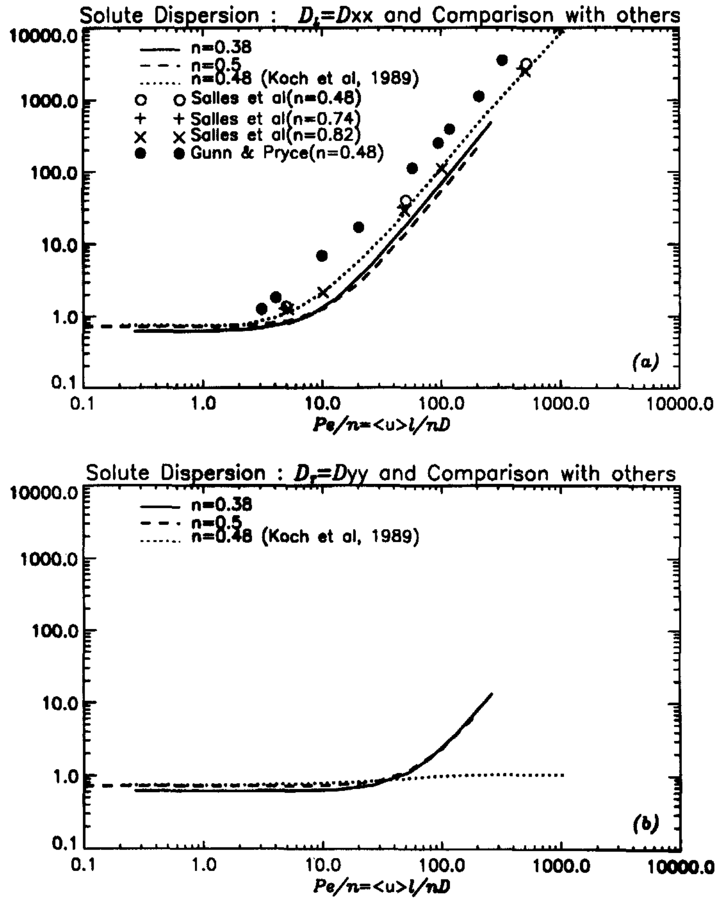

Fig. 3. The solute dispersion coefficients for the Wigner–Seitz grain and comparison with others; (a) the longitudinal dispersion coefficient D_L and (b) the transverse dispersion coefficient D_T.

array of uniform and insulated spheres with a porosity of 0.48, it is known that the effective conductivity is 0.344 [38]. Our numerical value for a Wigner–Seitz cell with porosity of 0.5 is 0.359 after multiplying the value 0.718 from Fig. 3(a) by the porosity to get the unit cell average. Obviously the small difference stems from different geometry. This provides a check for our numerical computation.

For large *Pe*, our numerical results D_L for Wigner–Seitz cell, as well as those by Salles *et al.* for uniform spheres, are consistent with the experimental measurements [37] and the analytical theory for dilute spheres [14]; all showing that D_L increases with Pe^2, when the mean flow is parallel to a lattice axis. (Recall from [14, 18] that if the flow is inclined to a lattice axis, D_L may vary linearly with *Pe*.) In contrast to the case of small *Pe*, the dependence on porosity is now reversed, and the dispersivity increases with decreasing porosity. Heuristically this is because the velocity gradient in the pores increases as porosity decreases and therefore enhances microscale mixing. The longitudinal dispersion coefficient for Wigner–Seitz cell is also compared in Fig. 4(a) and (b) with experimental data for natural granular media [39–45], all showing that D_L increases as the first power of *Pe*. Since the linear growth with *Pe* has been obtained in the models of random network of capillaries [8–11] and randomly and dilutely distributed spheres [12], the discrepancy of the power of *Pe* may in principle be removed by considering a microcell with many grains with varying sizes and random packing; the necessary computational task appears to be formidable, however.

The transverse dispersivity D_T computed for Wigner–Seitz grains is plotted in Fig. 3(b) for $Pe \leqslant 300$. Our computations could not yield accurate results for greater *Pe*. The qualitative trend is the same as D_L except that it is less than D_L by roughly two orders of magnitude. Mauri [46] also finds analytically for a dilute lattice of uniform spheres that D_T is proportional to Pe^2, for small *Pe* [46] and is eight times smaller than D_L. In contrast Koch *et al.* [14] predicts that D_T remains almost constant in *Pe* for very large *Pe*. There are no reliable measurements for D_T for a regular array of spheres. Some experimental data on D_T for natural granular media are available and are shown in Fig. 5(a) and (b) [43, 47–50]. Although scattered, each individual data set exhibits linear dependence on *Pe* as D_L. The discrepancy of D_T between the Wigner–Seitz grain and natural media is again probably due to randomness and size variation of natural grains.

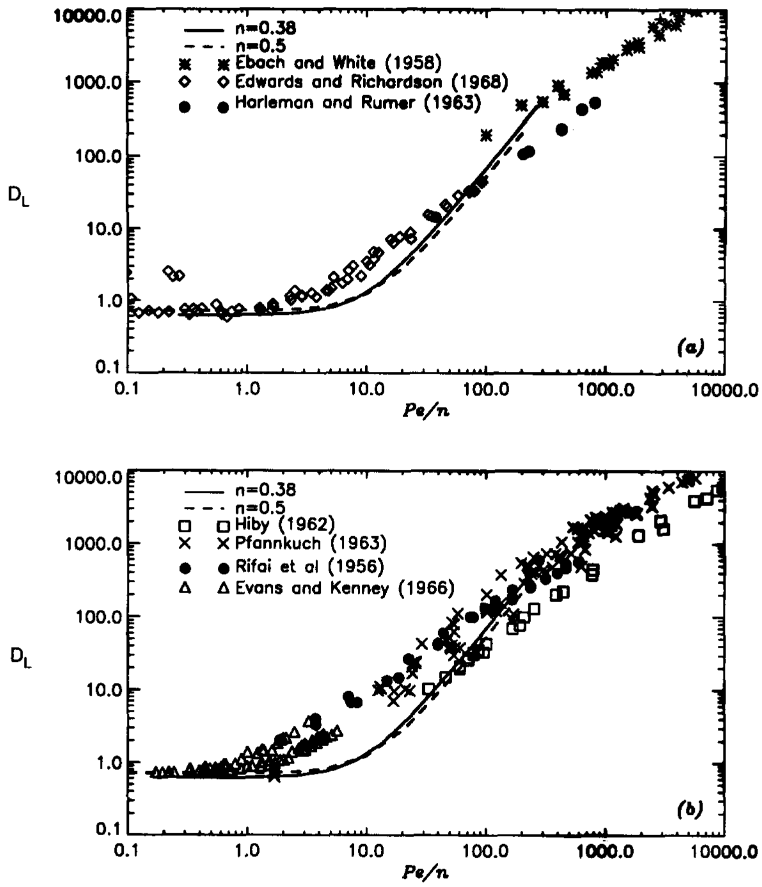

Fig. 4. Comparison of D_L for the Wigner–Seitz grain with experimental data for natural granular media.

COMPUTED DISPERSIVITY FOR HEAT

With the mean flow directed along the x-axis ($\theta = 0°$), the longitudinal and transverse dispersivities D_L and D_T for heat are plotted for Peclet numbers Pe up to 300 in Fig. 6 (a) and (b) for two porosities $n = 0.38$ and $n = 0.5$; the thermal properties for fluid and solid phases are assumed to be equal, i.e. $K_f = K_s$ and $\rho_f C_f = \rho_s C_s$. Also shown are some experimental results for randomly packed uniform glass spheres in water with roughly comparable thermal properties [51, 52].

In the limit $Pe = 0$, both D_L and D_T approach unity because the composite medium is homogeneous and there is no distinction between Ω_f and Ω_s for pure diffusion. For simple cubic packing of spheres with $n = 0.48$ and $K_s/K_f = 2$, Sangani and Acrivos [38] gives $D_T = 1.46$. As a check, we have also calculated the effective diffusivities with $n = 0.5$ and the same ratio of conductivities, and obtain $D_T = 1.458$. The small discrepancy is again due to different grain geometries.

In the relatively high Pe region, the dispersivities increase with decreasing porosity as in the case of passive solute (Fig. 6). This is again due to increased microscale mixing in the pore space caused by increased velocity gradient for smaller porosity value. The same trend has been observed for 2D array of cylinders in [26]. The experimental data for D_L in Fig. 6(a) show a growth of Pe^m where m has been estimated to be 1.256 in [51] and 1.4 in [52]. The discrepancy between theory and experiments must again be attributed to the difference in packings.

To see the effect of K_s/K_f, Fig. 7 shows D_L and D_T for two porosities ($n = 0.38, 0.5$) and two conductivity ratios, $K_s/K_f = 0$ and 1.† At the higher Peclet number, the longitudinal dispersivity D_L is greater, although the difference is small. This increase is due to heat diffusion through the solid phase. When the thermal gradient is in the direction of the mean flow, diffusion through the solid phase augments dispersion D_{xx} in the fluid when $K_s/K_f \neq 0$. But for D_{yy} which is associated with the thermal gradient normal to the flow, transverse dispersion is weakened by the loss of heat into solid. Quantitatively the effect of $K_s/K_f = 1$ on either D_L and D_T appears to be significant only at relatively low Peclet number, as shown in Fig. 7(a) and (b). This result is reasonable since for high Pe,

† We note that the results for $K_s/K_f = 0$ is the porosity n' times the dispersivity of the passive solute.

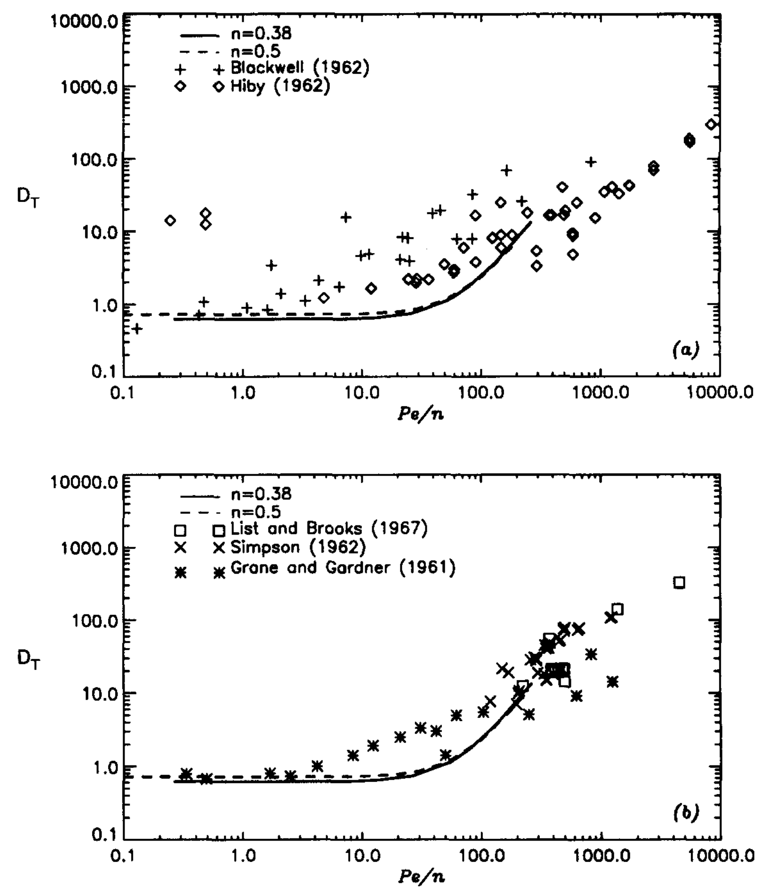

Fig. 5. Comparison of D_T for the Wigner–Seitz grain with experimental data for natural granular media.

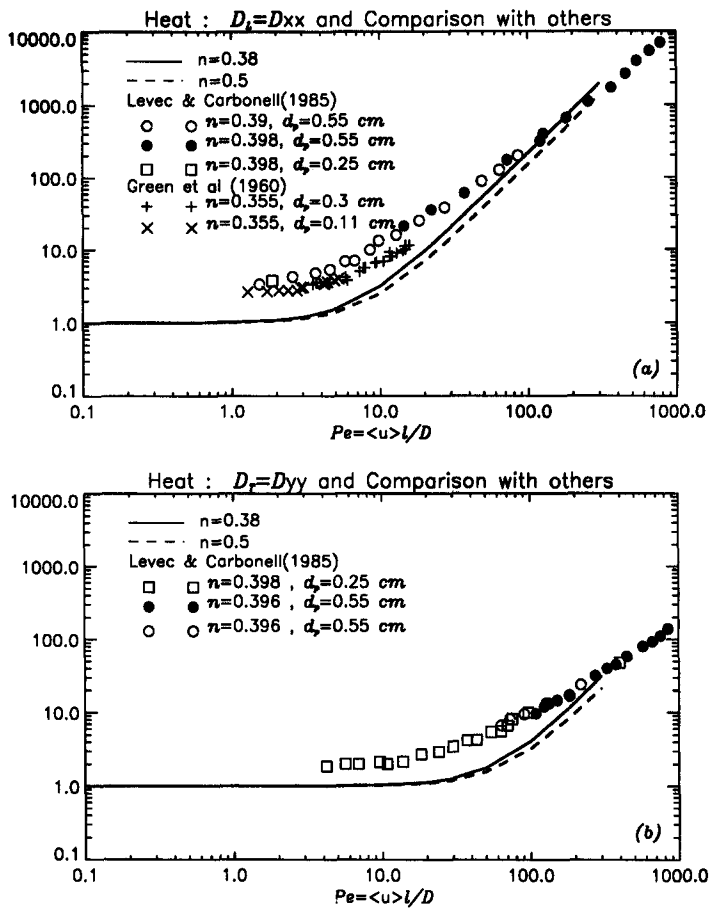

Fig. 6. Heat dispersion coefficients for the Wigner–Seitz grain with $\rho_s C_s/\rho_f C_f = 1$ and $K_s/K_f = 1$. (a) D_L and (b) D_T. In the cited experiments the thermal properties are $\rho_s C_s/\rho_f C_f = 0.9$ and $K_s/K_f = 1.7$ in Levec and Carbonell (1985) and $\rho_s C_s/\rho_f C_f = 0.52$ and $K_s/K_f = 1.7$ in Green *et al.* (1960).

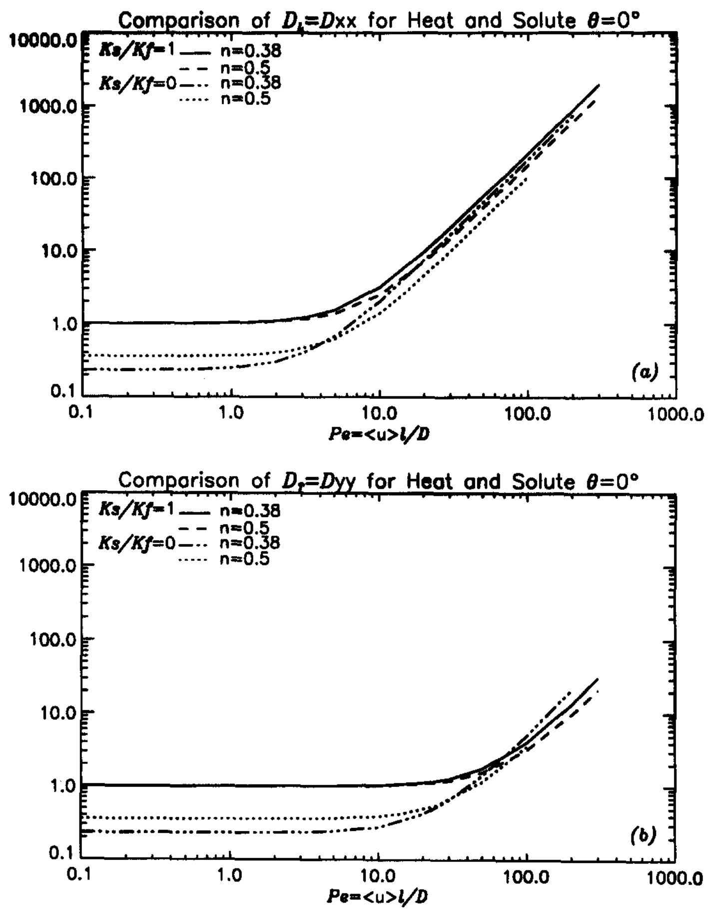

Fig. 7. Comparison of heat and solute dispersivities for the Wigner–Seitz grain for (a) D_L and (b) D_T.

dispersion by convection through the pore fluid must be dominant and diffusion in the solid must become immaterial.

In conclusion, we believe it to be important to conduct further numerical or analytical studies for micro-cells involving different grain sizes and random packing, for the understanding and prediction of flow and dispersion in porous media.

Acknowledgements—We are grateful for support from U.S. National Science Foundation through Grant MSM 8616693 by Solid and Geomechanics Program before July 31 1993 and Grant CTS 9115689 by Fluid Mechanics/Hydraulics/Particles Program after July 31 1993. We have also received additional supports from Air Force Office of Scientific Research, from Massachusetts Institute of Technology for a Research Initiation Grant and from U.S. National Science Foundation for using Pittsburgh Supercomputing Facility.

REFERENCES

1. H. Hasimoto, On the periodic fundamental solution of the Stokes equations and their application to viscous flow past a cubic array of spheres, *J. Fluid Mech.* **5,** 317–328 (1959).
2. A. S. Sangani and A. Acrivos, Slow flow through a periodic array of spheres, *Int. J. Multiphase Flow* **8**(4), 343–360 (1982).
3. A. A. Zick and G. M. Homsy, Stokes flow through periodic arrays of spheres, *J. Fluid Mech.* **115,** 13–26 (1982).
4. L. J. Snyder and W. E. Stewart, Velocity and pressure profiles for Newtonian creeping flow in regular packed beds of spheres, *A.I.Ch.E. J.* **12**(1), 167–173 (1966).
5. J. P. Sorensen and W. E. Stewart, Computation of forced convection in slow flow through ducts and packed beds—II. Velocity profile in a simple cubic array of spheres, *Chem. Engng Sci.* **29,** 819–825 (1974).
6. P. M. Adler, *Porous Media: Geometry and Transports.* Butterworth-Heinemann, London (1992).
7. H. Brenner, Dispersion resulting from flow through spatially periodic porous media, *Phil. Trans. R. Soc. Lond.* **297A,** 81–133 (1980).
8. D. J. de Jong, Longitudinal and transverse diffusion in granular deposites, *Trans. Am. Geophys. Un.* **39,** 67–74 (1958).
9. P. G. Saffman, A theory of dispersion in a porous medium, *J. Fluid Mech.* **6,** 321–349 (1959).
10. P. G. Saffman, Dispersion due to molecular diffusion and macroscopic mixing in flow through a network of capillaries, *J. Fluid Mech.* **7,** 194–208 (1960).
11. R. E. Haring and R. A. Greenkorn, A statistical model of a porous media with nonuniform pores, *A.I.Ch.E. J.* **16,** 477–483 (1970).
12. D. L. Koch and J. F. Brady, Dispersion in fixed beds, *J. Fluid Mech.* **154,** 399–427 (1985).
13. J. J. Fried and M. A. Combarnous, Dispersion in porous media, *Adv. Hydrosci.* **7,** 169–282 (1971).
14. D. L. Koch, R. G. Cox, H. Brenner and J. F. Brady, The effect of order on dispersion in porous media, *J. Fluid Mech.* **200,** 173–188 (1989).
15. M. Kaviany, *Principle of Heat Transfer in Porous Media.* Springer, Berlin. (1991).
16. R. G. Carbonell and S. Whitaker, Dispersion in pulsed systems—II. Theoretical developments for passive dispersion in porous media, *Chem. Engng Sci.* **38,** 1795–1802 (1983).
17. J. Rubinstein and R. Mauri, Dispersion and convection in periodic porous media, *SIAM. J. Appl. Math.* **46,** 1018–1023 (1986).
18. R. Mauri, Dispersion, convection and reaction in porous media, *Phys. Fluids* **3,** 743–756 (1991).
19. C. C. Mei, Heat dispersion in porous media by homogenization method, *Multiphase Transport in Porous Media,* ASME Winter Meeting, FED-Vol 122/HTD-Vol. 186, pp. 11–16 (1991).
20. C. C. Mei, Method of homogenization applied to dispersion in porous media, *Transport in Porous Media* **9,** 262–274 (1992).
21. H. Brenner and D. A. Edwards, *Macrotransport Processes.* Butterworth-Heinemann, London (1993).
22. H. Lee, Analysis of pseudo-continuum mass transfer in media with spatially periodic boundaries, *Chem. Engng Sci.* **34,** 503–514 (1979).
23. A. Eidsath, R. G. Carbonell, S. Whitaker and L. R. Herrmann, Dispersion in pulsed systems—III. Comparison between theory and experiments for packed beds, *Chem. Engng Sci.* **38,** 1803–1816 (1983).
24. R. A. Edwards, M. Shapiro, H. Brenner and M. Shapiro, Dispersion of inert solute in spatially periodic two-dimensional model porous media, *Transport in Porous Media* **6,** 337–358 (1991).
25. J. Salles, J.-F. Thovert, R. Delannay, L. Prevors, J.-L. Auriault and P. M. Adler, Taylor dispersion in porous media. Determination of the dispersion tensor, *Phys. Fluids* **5,** 2348–2376 (1993).
26. M. Sahraoui and M. Kaviany, Slip and no-slip temperature boundary conditions at the interface of porous, plain media: convection, *Int. J. Heat Mass Transfer* **37,** 1029–1044 (1994).
27. G. Burns, *Solid State Physics.* Academic Press, New York (1985).
28. A. Bensoussan, J. L. Lions and G. Papanicolaou, *Asymptotic Analysis for Periodic Structures.* North-Holland, Amsterdam. (1978).
29. E. Sanchez-Palencia, *Nonhomogeneous Media and Vibration Theory,* Lecture Notes in Physics, Vol. 127. Springer, Berlin (1980).
30. J. B. Keller, Darcy's law for flow in porous media by the two space method. *Nonlinear Partial Differential Equations in Engineering and Applied Sciences* (Edited by R. L. Sternberg, A. J. Kalinowski and J. S. Papadakis), pp. 429–443. Dekker, New York (1980).
31. C. C. Mei and J. L. Auriault, The effects of weak inertia on flow through a porous medium, *J. Fluid Mech.* **222,** 647–663 (1991).
32. H. Brenner and P. M. Adler, Dispersion resulting from flow through spatially periodic porous media—II. Surface and intraparticle transport, *Phil. Trans. R. Soc. Lond.* **307,** 149–200 (1982).
33. M. Sahraoui and M. Kaviany, Slip and no-slip temperature boundary conditions at interface of porous, plain media: convection—I. Formulation, *Proceedings of the* 1992 *National Heat Transfer Conference,* San Diego, California, HTD-Vol. 193, pp. 25–33 (1993).
34. B. M. Irons, A frontal solution program, *Int. J. Numer. Meth. Engng* **2,** 5–32 (1970).
35. P. C. Carman, Fluid flow through granular beds, *Trans Instn Chem. Engrs* **15,** 150–166 (1937).
36. J. Bear, *Dynamics of Fluids in Porous Media.* Elsevier, Amsterdam (1972).
37. D. J. Gunn and C. Pryce, Dispersion in packed beds, *Trans. Instn Chem. Engrs* **47,** T341–T350 (1969).
38. A. S. Sangani and A. Acrivos, The effective conductivity of a periodic array of spheres, *Proc. R. Soc. Lond. A* **386,** 262–275 (1983).
39. E. A. Ebach and R. R. White, Mixing of fluids flowing through beds of packed solids, *A.I.Ch.E. J.* **4**(2), 161–169 (1958).
40. M. F. Edwards and J. F. Richardson, Gas dispersion in packed beds, *Chem. Engng Sci.* **23,** 109–123 (1968).
41. E. V. Evans and C. N. Kenney, Gaseous dispersion in packed beds at low Reynolds numbers, *Trans. Instn Chem. Engrs* **44,** T189–T197 (1966).

42. D. R. F. Harleman and R. R. Rumer, Longitudinal and lateral dispersion in an isotropic porous medium, *J. Fluid Mech.* **16**(3), 385–394 (1963).
43. J. W. Hiby, Longitudinal and transverse mixing during single-phase flow through granular beds, *Proceedings of the Symposium on the Interaction Between Fluids and Particles*, London, 20–22 June, pp. 312–325 (1962).
44. H. O. Pfannkuch, Contribution a L'Etude des Deplacements de Fluides Miscibles dans un Milieu Poreux, *Revue de L'Institut Francais du Petrole*, **XVIII**(2), 215–270 (1963).
45. M. N. E. Rifai, W. J. Kaufman and D. K. Todd, Dispersion phenomena in laminar flow through porous media, Sanitary Engineering Research Laboratory and Division of Civil Engineering, University of California, Berkeley, Report No. 2, I. E. R. Series 93 (1956).
46. R. Mauri, Lagrangian self-diffusion of Brownian particles in periodic flow fields, *Phys. Fluids* **7**, 275–284 (1995).
47. R. J. Blackwell, Laboratory studies of microscopic dispersion phenomena, *Soc. Petroleum Engrs J.* **2,** 1–8 (1962).
48. F. E. Grane and G. H. F. Gardner, Measurements of transverse dispersion in granular media, *J. Chem. Engng Data* **6**(2), 283–287 (1961).
49. E. J. List and N. H. Brooks, Lateral dispersion in saturated porous media, *J. Geophys. Res.* **72**(10), 2531–2541 (1967).
50. E. S. Simpson, Transverse dispersion in liquid flow through porous media, *U.S. Geol. Surv. Prof.* Paper 411-C (1962).
51. J. Levec and R. G. Carbonell, Longitudinal and lateral thermal dispersion in packed beds—II. Comparison between theory and experiment, *A.I.Ch.E. J.* **31,** 591–602 (1985).
52. D. W. Green, R. H. Perry and R. E. Babcock, Longitudinal dispersion of thermal energy through porous media with a flowing fluid, *A.I.Ch.E. J.* **10**(5), 645–651 (1960).